Mathematical Oncology

Quantitative Metrics of Net Proliferation and Invasion Link Biological Aggressiveness Assessed by MRI with Hypoxia Assessed by FMISO-PET in Newly Diagnosed Glioblastomas

Mindy D. Szeto,[1] Gargi Chakraborty,[1] Jennifer Hadley,[1] Russ Rockne,[1] Mark Muzi,[2] Ellsworth C. Alvord, Jr.,[1] Kenneth A. Krohn,[2] Alexander M. Spence,[3] and Kristin R. Swanson[1]

Departments of [1]Pathology, [2]Radiology, and [3]Neurology, University of Washington School of Medicine, Seattle, Washington

Abstract

Glioblastoma multiforme (GBM) are aggressive and uniformly fatal primary brain tumors characterized by their diffuse invasion of the normal-appearing parenchyma peripheral to the clinical imaging abnormality. Hypoxia, a hallmark of aggressive tumor behavior often noted in GBMs, has been associated with resistance to therapy, poorer survival, and more malignant tumor phenotypes. Based on the existence of a set of novel imaging techniques and modeling tools, our objective was to assess a hypothesized quantitative link between tumor growth kinetics [assessed via mathematical models and routine magnetic resonance imaging (MRI)] and the hypoxic burden of the tumor [assessed via positron emission tomography (PET) imaging]. Our biomathematical model for glioma kinetics describes the spatial and temporal evolution of a glioma in terms of concentration of malignant tumor cells. This model has already been proven useful as a novel tool to dynamically quantify the net rates of proliferation (ρ) and invasion (D) of the glioma cells in individual patients. Estimates of these kinetic rates can be calculated from routinely available pretreatment MRI *in vivo*. Eleven adults with GBM were imaged preoperatively with ^{18}F-fluoromisonidazole (FMISO)–PET and serial gadolinium-enhanced T1- and T2-weighted MRIs to allow the estimation of patient-specific net rates of proliferation (ρ) and invasion (D). Hypoxic volumes were quantified from each FMISO-PET scan following standard techniques. To control for tumor size variability, two measures of hypoxic burden were considered: relative hypoxia (RH), defined as the ratio of the hypoxic volume to the T2-defined tumor volume, and the mean intensity on FMISO-PET scaled to the blood activity of the tracer (mean T/B). Pearson correlations between RH and the net rate of cell proliferation (ρ) reached significance ($P < 0.04$). Moreover, highly significant positive correlations were found between biological aggressiveness ratio (ρ/D) and both RH ($P < 0.00003$) and the mean T/B ($P < 0.0007$). [Cancer Res 2009;69(10):4502–9]

Major Findings

Overall, biological aggressiveness assessed by serial MRI is linked with hypoxic burden assessed on FMISO-PET using a novel biomathematical model for glioma growth and invasion. This study suggests that patient-specific modeling of growth kinetics can provide novel and valuable insight into the quantitative connections between disparate information provided by multimodality imaging.

Introduction

Gliomas are uniformly fatal lesions of the brain signified by their invasive potential and their increased capacity for proliferation (1). This is especially true of glioblastoma multiforme (GBM; WHO grade 4); a highly anaplastic, rapidly proliferating, primary brain neoplasm characterized by diffuse invasion of the normal-appearing parenchyma peripheral to the abnormality seen on clinical imaging. As outlined by Stupp and colleagues (2, 3), the current standard-of-care for newly diagnosed GBMs involves resection followed by adjuvant radiation and chemotherapy. However, GBMs typically recur within months, with a poor prognosis of 6 to 14 months (4).

Magnetic resonance imaging (MRI) and positron emission tomography (PET) can offer noninvasive means to assess individual tumor biology *in vivo*, thereby assisting diagnosis as well as patient-specific treatment planning. MRI provides anatomic tumor information by allowing visualization of the lesion's structural extent. Gadolinium enhancement on T1-weighted MRI (T1Gd MRI), allows the bulk tumor mass to be imaged, with hyperintense-appearing neoangiogenesis enclosing a hypointense region of central necrosis or dead tissue. T2-weighted MRI (T2 MRI) detects the surrounding edema associated with invading glioma cells.

Recent developments in radiopharmaceutical research has produced PET tracers that can target hypoxia, among other characteristic errors of disease (5–8). Imaging with radiolabeled nitroimidazoles offers a noninvasive means of assessing hypoxia. One of the earliest and most commonly used agents for hypoxia detection was the PET tracer ^{18}F-fluoromisonidazole (FMISO), a nitroimidazole derivative (9, 10). Nitroreductases within the cell metabolize nitroimidazoles, which can act as electron acceptors when oxygen levels are low. Reduced nitroimidazoles covalently bond to intracellular macromolecules and cannot exit viable cells,

Requests for reprints: Kristin R. Swanson, Laboratory of Neuropathology, University of Washington, 325 9th Avenue, Box 359791, Seattle, WA 98104. Phone: 206-221-6577; Fax: 206-685-7271; E-mail: swanson@amath.washington.edu.

doi:10.1158/0008-5472.CAN-08-3884

Quick Guide: Main Model Equations

Equation 1:

$$\overbrace{\frac{\partial c(x,t)}{\partial t}}^{\text{rate of change of glioma cell density}} = \overbrace{\nabla \cdot [D(x)\nabla c]}^{\text{net dispersal of glioma cells}} + \overbrace{\rho c\left(1-\frac{c}{k}\right)}^{\text{net proliferation of glioma cells}}$$

This is a reaction-diffusion partial differential equation used to describe the density of glioma cancer cells (c) in terms of two net rates: motility (D) and proliferation (ρ). The equation relates the temporal rate of change of glioma cell density at the spatial location x with the diffuse motility of the cancer cells near that location and the net cell proliferation of those cells locally. The net motility rate D varies depending on the location in the brain to allow for an increased velocity of migration through white matter compared with gray matter. The (maximum) net proliferation rate ρ includes both birth and death rates and assumes logistic growth with a tissue-carrying capacity k. There is a spatial heterogeneity in the net proliferation term resulting from the effect of k. At the center of a densely packed tumor, the net proliferation term becomes 0 with a gradient to a local maximum rate of ρ for those diffusely invading cells at the periphery. Although local proliferation rates at the microscopic level will vary depending on genetic and molecular mechanisms, by considering net proliferation ρ, the model attempts to capture the downstream effects of these mechanisms on the tumor cell population as a whole.

Major Assumptions of the Model

This model assumes that glioma cell invasion throughout the brain is a diffusion process and that the coefficient of diffusion (D) can vary in space depending on the gray and white composition of the brain at that location. The model also assumes logistic growth of the tumor cell population, so that the net proliferation rate (ρ) is lower in regions of high cell density (where $c \approx k$) than in regions of low cell density (where $c \ll k$).

such that FMISO uptake is proportional to the amount of hypoxia (11). This does not occur in necrotic tissues due to a lack of enzyme activity, which is required for the metabolic processing of bioreductive probes.

GBMs are characterized by hypoxia, which results from the rapid depletion of nutrients that occurs with aberrant tumor cell proliferation (12). Hypoxia has been shown to be associated with the propagation and progression of malignant tumors (13), as well as being a predictor of resistance to standard radiotherapy and some varieties of concurrent chemotherapy (14). Accordingly, tumors with significant levels of hypoxia generally show a lower probability of remaining asymptomatic, as well as shorter overall survival (11, 15). By limiting tumor response to and control by therapy, hypoxia is an important adverse prognostic factor that is indicative of higher rates of recurrence and fatality. Additionally, the related necrosis is characteristic of GBM diagnoses (16). It has been suggested that the hypoxia-stimulated expression of genes for oncoproteins, glucose transporters, and glycolytic enzymes confers a growth advantage for the tumor and allows hypoxic cells to use the energy-saving mechanism of glycolysis (17), which may promote a more aggressive tumor phenotype.

Given the high degree of invasiveness and the inability of current medical imaging technology to capture the full extent of glioma invasion, biomathematical modeling has been used to shed light on the growth patterns of gliomas *in vivo*. The mathematical model developed by Swanson and colleagues (18–20) describes growth and invasion in terms of two patient-specific variables: the net cell dispersal rate (D) and proliferation rate (ρ). See the Quick Guide for further details. The model considers the expansion of MRI-detectable edge of the tumor as resembling a traveling wave that asymptotically approaches a constant velocity $v = 2\sqrt{D\rho}$ (21–23). In untreated gliomas, linear radial growth has been observed (24, 25). Furthermore, Pallud and colleagues (26) established that the model-predicted constant velocity (contributed to by both D and ρ) of low-grade glioma growth is a prognostic factor. Similarly, kinetic analyses of tumor growth have shown that untreated gliomas grow continuously at predictable rates before their inevitable progression to more malignant phenotypes. Growth velocity has also been seen to predict the conversion to contrast-enhancement on MRI (27). The model parameters for biological aggressiveness (D and ρ) have prognostic significance even when controlling for standard clinicopathologic parameters.[4] A simulated example based on patient-specific values for D and ρ is provided in Fig. 1, along with a comparison of representative multimodality patient images from which D and ρ can be obtained.

Given the successful application of this model to characterizing glioma kinetics in terms of net rates of proliferation and invasion, it is appropriate to explore how hypoxic burden, a hallmark of aggressive tumor behavior, relates to the model parameters that can be used as quantitative measures of biological aggressiveness. Given the model-defined biological aggressiveness metrics for each patient, this study investigates the link between anatomic glioma growth kinetics assessed on MRI and hypoxic burden as seen on FMISO-PET.

Materials and Methods

Patients. Eleven adult patients with newly diagnosed GBM were imaged preoperatively with FMISO-PET, T1Gd, and T2 MRI sequences. There were seven males and four females, with ages ranging from 37 to 73 (median, 55; mean, 57.6). Karnofsky performance scores at diagnosis ranged from 60 to 90 (median, 70; mean, 74). These patients were recruited from the University of Washington Medical Center. Each patient signed informed consent for inclusion in our study, with prior approval by the Institutional Review Board and Radiation Safety committees.

FMISO-PET imaging protocol. FMISO was prepared as outlined by Lim and Berridge (28) and detailed methods are described elsewhere (29). Briefly, all PET scans were performed on an Advance Tomograph (G.E. Medical Systems) operating in a three-dimensional, high-resolution mode with 35 imaging planes covering a 15-cm axial field of view. For each patient, venous access lines were placed in each arm, one for FMISO

[4] C.H. Wang, J.K. Rockhill, M. Mrugala, et al. Prognostic significance of growth kinetics in newly diagnosed glioblastomas revealed by combining serial imaging with a novel biomathematical model. Cancer Res. Submitted 2008.

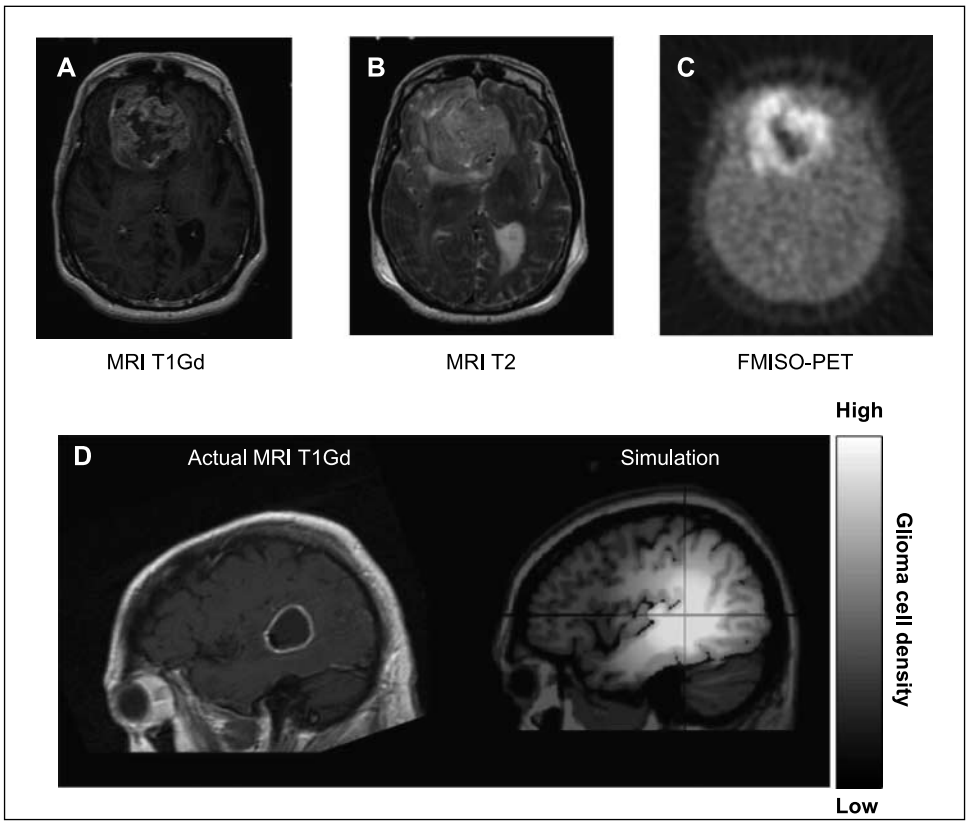

Figure 1. A 55-year-old woman with a temporal GBM imaged preoperatively on T1Gd MRI (*A*), T2 MRI (*B*), and FMISO-PET (*C*). MRI showed a contrast-enhancing tumor with a large necrotic center. A simulation of tumor expansion (*D*) was generated by applying D and ρ measured from the serial MRI of a ring-shaped temporal glioblastoma, revealing a diffuse extent of disease peripheral to the imaging abnormality.

injection and the other for blood sampling. Injections of 3.7 MBq/kg (0.1 mCi/kg) of FMISO were then administered, for a maximum of 260 MBq or 7 mCi. A single field-of-view emission scan from 120 to 140 min postinjection and an attenuation scan (25 min) of the brain with tumor were obtained. The acquired imaging data were reconstructed to determine the tumor hypoxic volume (HV) as described in later sections. During emission tomography, four venous blood samples were obtained at intervals of 5 min. Whole blood samples of 1 mL each were counted in a Cobra multichannel gamma well counter (Packard Corp.) that is calibrated each week in units of cpm/MBq. Blood activity of the four samples was averaged and then expressed as MBq/mL of decay corrected to time of injection.

MRI protocol. MRIs were acquired using a 1.5 T G.E. system (Horizon LX Echospeed with 9.1 software). The preoperative Stealth navigation studies included axial T1 with contrast (three-dimensional gradient echo, TE/TR minimal, 1.3 mm slice thickness with no skip, FOV 26), and axial T2 FSE (TE 97.3, TR 4000, 1.7 mm slice thickness with no skip, FOV 26). Follow-up scans including standard gadolinium-enhanced T1-weighted (TE minimal, TR 350) and T2-weighted (TE 102, TR 4300) MRIs were obtained in two-dimensional mode with a spin echo sequence and slice thickness of 5 mm with no interslice spacing.

Image processing and data acquisition. The number of days between the FMISO-PET and MR images ranged from 0 to 16 with an average of 7.2 days. Spatial registration of the T2 MRI and the FMISO images to the T1Gd MRI was performed using Statistical Parametric Mapping software (30) in order to compare regions of PET activity relative to MRI-defined abnormalities. The accuracy of image coregistration was confirmed by visual inspection in addition to the optimization features provided by Statistical Parametric Mapping.

Data acquisition from FMISO-PET and MRIs was performed with a semiautomated image-processing program developed in MATLAB (31), which consisted of three parts: MRI (T1Gd and T2) thresholding, FMISO-PET thresholding, and computational determination of different tumor regions of a glioma. Specific details of the techniques used are reported elsewhere (29).

The coregistered FMISO-PET images were scaled to the average venous blood concentration of FMISO activity to produce tumor/blood (T/B) values. This allowed for a three-dimensional pixel-by-pixel calculation of T/B activity ratios.

The number of pixels in the brain with a T/B ratio of $\geq$1.2, indicating hypoxia, was determined and converted to milliliters to give the HV. T/B ratios previously measured with the tomograph in normal brain and muscle showed that >90% of the values decreased to <1.1 (32), and our cutoff ratio of 1.2 was in accordance with previous studies (9). Due to the nature of PET imaging, small nontumorous regions of FMISO activity are typically scattered in isolated voxels throughout the brain. Designating HV as FMISO T/B $\geq$ 1.2 largely excludes this noise, and is also consistent with results from histologic and immunohistochemical definitions of the hypoxic region. To normalize hypoxia for tumors of different sizes, we defined relative hypoxia (RH) by scaling the HV, as determined on FMISO-PET, to the T2-weighted MR-defined volume, giving the unitless hypoxic fraction RH = HV/T2 volume. Because FMISO-PET is not retained in necrotic tissue, we also considered an alternate measure of relative hypoxia, termed RH*, defined as the HV normalized to the volume of the nonnecrotic T2 region (thus removing the central hypointensity on T1Gd).

Although the choice of a T/B cutoff of 1.2 is consistent with previous studies exploring FMISO-PET (9, 12, 29), we chose to consider a variety of possible T/B cutoffs to assure that our findings were not as a result of this relatively arbitrary cutoff choice. First, FMISO-PET images for each patient were scaled using a range of T/B ratios (0.9–1.6). Values for HV (associated with each new cutoff choice) and the resultant RH were then obtained.

The analysis focuses on the association between the model parameters and RH, which we believe is a more accurate and biologically based quantification of the tissue's hypoxic burden, which controls for the overall size of the region in which hypoxia may be imaged. It would be inappropriate to compare rates (of biological aggressiveness) with volumes (e.g., HV) because the tumors are imaged at various times during their evolution. Moreover, the growth rate can be independent of size. Additionally, we considered the average T/B intensity of pixels at or above

the 1.2 threshold as a measure of hypoxic density, denoted as mean T/B in our analysis. Examining the relationships between the model parameters and mean T/B allows for a complementary characterization of hypoxic burden.

Calculation of model parameters. Following Swanson and colleagues (18–20), for contrast-enhancing gliomas, the biomathematical model allows for the calculation of the ratio of the net proliferation rate ρ to the net dispersal coefficient D (ρ/D) from a single pair of T1Gd and T2 sequences. A second sequence of MR images without intervening treatment was available for a subset of the patients included in this study ($n = 5$), which allowed the explicit definition of the two unknown variables, D and ρ, in individual patients. The velocity of radial expansion v was also determined for those cases.

Tumor sphericity. Previous work on cell-based mathematical modeling of tumor invasion has linked more aggressive cellular phenotypes with the formation of masses with finger-like protrusions (33). Furthermore, these modeling approaches have found that hypoxia can select for these more aggressive phenotypes. We also examined the degree of sphericity in our three-dimensional analysis of each tumor to provide an additional spatial metric of growth kinetics and aggression. Sphericity (Ψ) was calculated relating the surface area (SA, cm^2) with the volume (V, cm^3) of each tumor on a scale from 0 to 1: $\psi = \frac{\pi^{1/3}(6V)^{2/3}}{SA}$. This three-dimensional geometric index has been applied to measure a tumor's similarity to a spherical object (34), in which a sphericity value of 1 indicates that the tumor is perfectly spherical, and values less than 1 signify a more irregular and fingered shape. As the compactness measure of a three-dimensional shape, sphericity decreases with the amount of surface area. This measure was quantified for both T1Gd and T2 images (Table 1).

Statistical analysis. Pearson correlation was used to assess the association between the model parameters and hypoxic burden, with the P value for statistical significance determined using Student's t distribution.

Results and Discussion

All patients had GBM as designated by WHO criteria (35). The patient age, sex, Karnofsky performance score at diagnosis, HV, RH, velocity of glioma expansion, the computed values of the model parameters D and ρ, and the ratio ρ/D are shown in Table 1. Values for v, D, and ρ are displayed for five patients for whom two imaging studies were available over a period of time prior to any operation or treatment.

Correlates of hypoxic burden and net proliferation/diffusion. The statistical significance of associations between hypoxic burden and the MRI-defined anatomic tumor burden quantified by v, D, and ρ are summarized in Table 2. A significant (Pearson) correlation was found between the net rate of cell proliferation (ρ) and RH ($P < 0.04$), as well as RH* ($P < 0.04$). Correlations with dispersal (D) did not reach significance. The mathematical model and our traveling wave approximation of glioma expansion suggest that both ρ and D contribute to v. The velocity, v, only approached significance when compared with RH.

In the context of hypoxia, model-defined biological aggressiveness may also be quantitatively assessed by the ratio ρ/D based on the observation that a cell population with increased proliferation (ρ) relative to invasive capability (D) would be more likely to produce local hypoxia. The ratio ρ/D can be related to the gradient of the leading (invading) edge of the tumor. That is, a high ρ/D would correspond to a mitotically active (high ρ) tumor with relative low invasiveness (low D) leading to a relatively well-demarcated nodule. Conversely, a low ρ/D would correspond to a diffusely invasive leading-edge of the tumor consistent with a tumor that has a relatively lower proliferative capacity compared with its diffuse invasion. We did note a consistent pattern for which a larger ρ also suggested a larger D, such that ρ/D also increased. The biological aggressiveness ratio ρ/D showed strong correlation with RH ($P < 0.00003$) and RH* ($P < 0.00002$). In addition, ρ/D was found to significantly correlate with mean T/B ($P < 0.0007$).

Correlates of tumor sphericity. In response to a number of computational studies suggesting that the tumor microenvironment (e.g., local hypoxia) can drive the formation of tumors that are less spherical (33), we explored the tumor sphericity as an alternate candidate measure of tumor aggressiveness. Correlation analysis was performed between sphericity and all glioma growth characteristics quantified through anatomic and functional imaging. Sphericity on T1Gd negatively correlated with RH ($P < 0.04$), mean T/B ($P < 0.02$), and ρ/D ($P < 0.009$). Pearson correlation results for sphericity delineated on T2 also reached significance for mean T/B ($P < 0.05$) and ρ/D ($P < 0.008$).

Alternative T/B ratios. Based on the hypothesis that hypoxia would not be expected at large distances from the bulk tumor

Table 1. Patient age, sex, performance status, HV (T/B $\geq$ 1.2), RH, mean T/B, velocity of growth v, dispersal D, cell proliferation ρ, and circularity on T1Gd and T2 MRI

No.	Age	Sex	KPS	T1Gd volume (cm^3)	T2 volume (cm^3)	HV (cm^3)	RH	Mean T/B	Velocity (mm/y)	D (mm^2)	ρ (1/y)	ρ/D ($1/mm^2$)	Sphericity T1Gd	Sphericity T2
1	54	F	60	39.5	94.3	120.5	1.28	1.49	—	—	—	0.75	0.43	0.57
2	73	M	60	23.6	75.9	75.2	0.99	1.56	—	—	—	0.53	0.83	0.68
3	55	F	70	79.8	166.8	180.9	1.08	1.65	—	—	—	0.66	0.44	0.54
4	72	M	70	14.4	38.1	123.8	3.25	1.74	—	—	—	1.17	0.35	0.48
5	37	M	90	50.8	177.9	33.7	0.19	1.41	6.5	6.3	1.7	0.27	0.73	0.94
6	63	M	90	30.4	78.1	119.2	1.53	1.53	95.6	55.3	41.3	0.75	0.39	0.38
7	43	M	70	25.4	111.5	28.8	0.26	1.37	—	—	—	0.29	0.61	0.75
8	56	M	100	39	152.6	63.4	0.42	1.48	—	—	—	0.26	0.78	0.81
9	54	F	70	8.4	44.9	52.5	1.17	1.28	96.7	72.3	32.4	0.45	0.86	0.86
10	53	F	70	2.6	37.8	19.2	0.51	1.37	32.1	28.9	8.9	0.31	1.07	1.01
11	70	M	70	16.4	66.9	6.3	0.09	1.26	48.6	36.9	16	0.43	0.92	0.53

Abbreviation: KPS, Karnofsky performance score.

Table 2. P values and R^2 for the correlations of FMISO-determined measures of hypoxic burden (RH and mean T/B) and MR-defined growth characteristics (v, D, and ρ)

		P	R^2
RH vs	Velocity, v (mm/y)	0.057	0.75
	D (mm^2)	0.12	0.6
	ρ (1/y)	0.034*	0.82*
	ρ/D (y/mm^2)	0.000021*	0.88*
RH* vs	Velocity, v (mm/y)	0.055	0.76
	D (mm^2)	0.12	0.6
	ρ (1/y)	0.03*	0.83*
	ρ/D (y/mm^2)	0.000018*	0.88*
Mean T/B vs	Velocity, v (mm/y)	0.18	0.5
	D (mm^2)	0.31	0.33
	ρ (1/y)	0.11	0.62
	ρ/D (y/mm^2)	0.00069*	0.74*

NOTE: Asterisks indicate associations reaching statistical significance ($P < 0.05$).

mass, for each T/B cutoff, an associated HV was calculated and the portion of that HV residing beyond the tumor region was graphed (data not shown). The results showed that the HV occupying presumed nontumorous regions precipitously declined around the 1.2 level, indicating that the FMISO activity at or above the T/B = 1.2 level is largely restricted to previously defined areas of MRI abnormality. More than 99% of normal-appearing brain in the hemisphere contralateral to the tumor was observed to have a T/B of <1.2. Figure 2 of a right frontal GBM displays a graphical example of an FMISO-PET image subjected to thresholding at each of the T/B levels considered. These data support the reasonability of using the 1.2 T/B level as a threshold for hypoxia.

For each patient, RH plots were generated against various threshold levels ranging from 0.9 to 1.6 in increments of 0.1, yielding the results summarized in Fig. 3. RH decreased somewhat linearly as the ratio increased, as expected. Of special note is our observation that the value for the ratio ρ/D increases as a function of RH, regardless of the T/B level used. This suggests that the hypothesized "ideal" T/B = 1.2 is not a confounding factor in considering hypoxic burden as a marker of a tumor's biological aggressiveness. The striking linearity of the scatter of the MRI-defined ρ/D relative to RH is illustrated in Fig. 4. The positive relationship holds regardless of T/B threshold, which further confirms our conclusion from the results depicted in Fig. 3.

Conclusions

Hypoxia is a clinically important feature of glioblastomas, specifically as it relates to treatment resistance. The ability of FMISO-PET to visualize and quantify the hypoxic fraction of the tumor is highly relevant in clinical applications. Although the gold standard for distinguishing hypoxia is often considered to be direct measurement of pO_2 levels with electrodes, this technique is practically and ethically impossible for the routine monitoring of hypoxia in intracranial tumors, as the procedure must be performed intraoperatively. Previous literature has established the utility of FMISO-PET in the noninvasive assessment of hypoxia (36) and has been linked to pO_2, in which FMISO retention is detectable in the range of $\leq$2 to 3 mm Hg (10, 37, 38). For cancers of the head and neck, it has been shown that hypoxia (imaged via FMISO-PET) can affect prognosis independently of other prognostic variables (39). Although there is evidence that the association between hypoxia and clinical outcome may not hold across glioma grades (40), recent multivariate analyses of GBM patient survival revealed significant correlations with the volume of FMISO-PET imageable hypoxia alone (9).

Assessing the spatiotemporal growth of GBM through a biomathematical model that is driven by patient-specific variables offers a novel means of connecting overall growth kinetics (visible on MRI) to the hypoxia-guided resistance mechanism (visible on FMISO-PET). Previous analysis of this model relate the radial velocity of tumor growth to survival (41), and show that this variable predicts the conversion of non–contrast-enhancing low-grade gliomas to contrast-enhancement on T1Gd MRI (27). These results imply that our biomathematical model accurately predicts the growth of untreated tumors over time and can distinguish between the growth of variably aggressive tumors. Combining these results with conclusions from other studies that define hypoxic conditions as an important feature of aggressive tumor microenvironment (33) lead us to investigate the relation between tumor aggressiveness quantified through our model parameters and aggressive phenotype associated with hypoxia that can be imaged by FMISO-PET for human GBMs.

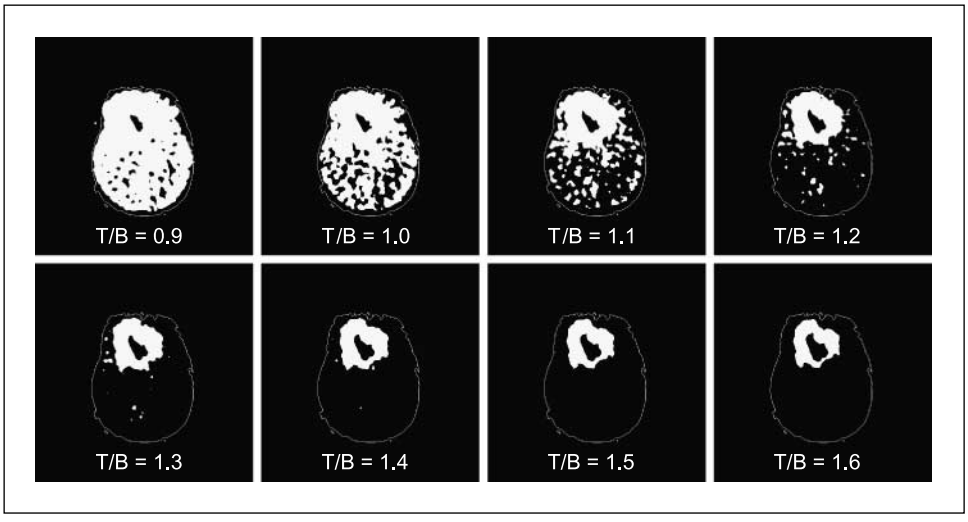

Figure 2. An illustration of the results of applying a range of T/B ratios to the FMISO-PET image of a right frontal GBM (patient no. 3) to generate visualizations of the HV regions suggesting that T/B = 1.2 is a reasonable threshold to define a HV separate from imaging noise.

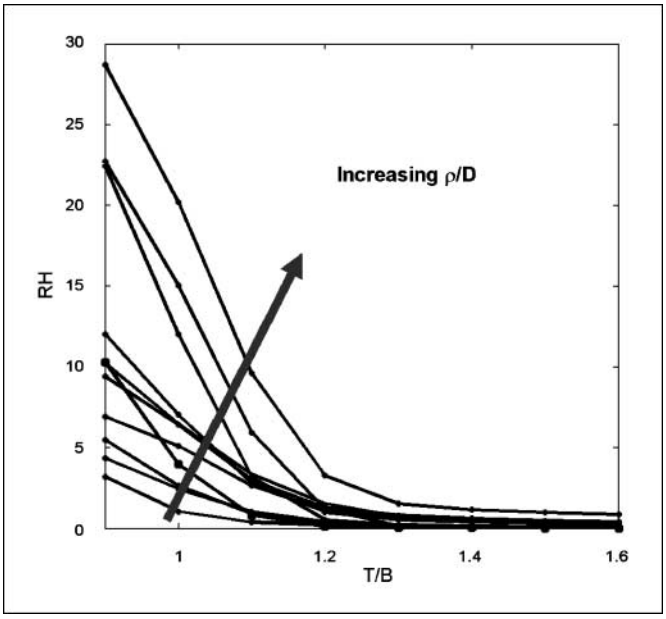

Figure 3. Plot of RH as measured at various T/B thresholds. Curves represent individual patients (n = 11), with the direction of the superimposed arrow denoting a general increase in ρ/D values.

The positive relationship between the model parameters and hypoxic burden is consistent with our current understanding of the process by which hypoxia arises. That is, highly proliferative tumors (high ρ) are thought to be more likely to be hypoxic with some recent PET imaging to support this *in vivo* (42). Furthermore, intuitively, those invasive gliomas for which there is a high net proliferation rate relative to the net invasion rate (ρ/D) would likely form a hypoxic microenviroment based on the relative time rate for depletion of resources (e.g., oxygen via increasing cell numbers via proliferation) relative to the ability of the population of glioma cells to migrate away from the potentially hypoxia-forming environment. Although this is an intuitive concept in overall population dynamics, the positive correlation of the ratio of the net proliferation and the net invasion rate (ρ/D) with the resultant RH, RH*, and mean T/B concurs with our hypothesis that hypoxia is a hallmark of aggressive tumor behavior.

This significant correlation between the model parameters for biological aggressiveness and the hypoxic burden assessed by RH, RH*, and mean T/B persists across a wide range of T/B threshold values used for defining the HV. When choosing ratios below 1.2, there tends to be significant overlap of the histogram of T/Bs from contralateral normal brain and tumor regions, whereas ratios above 1.2 tend to provide for clear delineation between the normal brain and (hypoxic) tumor tissue. We explored varying the T/B cutoff across all patients to confirm that the results relating the hypoxic burden assessed at cutoff 1.2 did not significantly change the results. Because FMISO-PET has been shown to correlate with the pO_2, increasing the hypoxic threshold to levels above 1.2 would correspond to selecting regions of that tumor that are increasingly hypoxic. Thus, our results suggest that at every magnitude of hypoxia (T/B $\geq$ 1.2), the biological aggressiveness assessed by the biomathematical model and MRI correlates significantly with hypoxic burden assessed by FMISO-PET.

Previous cell-based computational models of tumor growth and invasion have shown that hypoxic environments can select for cells with aggressive phenotypes, which give rise to fingered-tumor morphologies that have low sphericity *in vitro* (33). This suggests that when more aggressive tumor clones are selected, the tumor growth pattern is more "bumpy." To expand on these

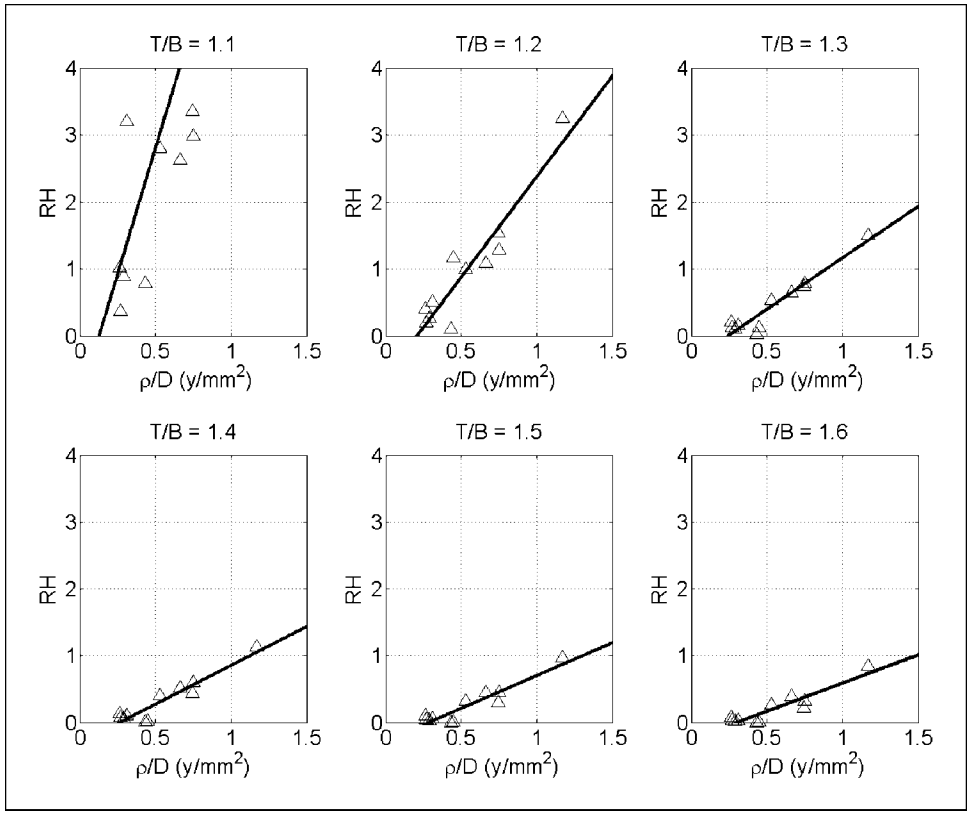

Figure 4. Scatter plots of RH versus ρ/D for all patients in this study (n = 11). RH was determined over a variety of T/B levels, ranging from 1.1 to 1.6 in increments of 0.1. A strong linear relationship between the variables is shown for all thresholds; correlations were statistically significant for all T/B levels considered.

computational and experimental studies, we quantitatively investigated the association of clinically observed sphericity on MRI with hypoxia and the model parameters. Inverse correlation of tumor sphericity with RH and mean T/B imply that more fingered or abnormally shaped tumors tend to have greater hypoxic burden. Large ρ/D correlates with low sphericity, which suggests extensive infiltration and a high grade of tumor cell dissociation. The observed results are therefore the first to provide clinical-scale support for existing theoretical cell-based models which suggest that aggressive cell lines produce tumors that may be less spherical (33). This is a novel insight that suggests further investigation as there are many differences between the computational models that were originally suggestive of this less spherical growth pattern and the models used here to quantify aggressiveness.

This report suggests a means of quantifying the *in vivo* biological link between the hypoxic burden of the tumor and the overall growth characteristics of individual gliomas. The validated mathematical model we have used in this study is a unique tool towards this end, as it is able to quantitatively connect the overall aggressive behavior (ρ/D) of a tumor assessed on MRI to that assessed on FMISO-PET as hypoxia, a biological result of its microenviroment. These results argue that FMISO-PET measurement in untreated GBM are able to quantify an essential outcome variable and can extend our understanding of an important pathophysiologic process beyond what is shown by conventional anatomic imaging.

Further investigation is necessary to clarify these links between anatomic and functional imaging, due in part to the small sample size used in this study, as well as the brief time scale over which preoperative imaging data is obtained. In light of the present data, it may be possible that brain tissue heterogeneity and the placement of anatomic structures in relation to individual tumors may have affected our results. In retrospect, however, the general scarcity of data available for analysis highlights the bleak clinical reality of glioblastoma. It follows that a precise, biologically based method to better understand its growth kinetics is highly necessary.

It is important to note that cancer modeling is dictated by biology, not the mathematics. As noted previously, the biomathematical model used in this study attempts to capture the downstream effects of the tumor microenvironment. Variables can be considered individually or together to assess their biological significance and testability. A striking advantage of this patient-specific model is that its predictions are readily personalized through the determination of only two key variables; this parsimonious approach is reflected throughout much of current modeling research (43). However, we realize that there are limitations to such a mathematical formulation for aggressiveness. Although the parameters consider tumor growth as an expansion of its traveling wave front, other factors can combine to determine the patient's overall clinical outcome, notably prognostic factors include age and Karnofsky performance score, which are of a more stochastic phenomena lacking a sufficiently understood underlying mechanism that can be incorporated into the model. But developing a mathematical model is an iterative process; upon comparison to clinical results, the model can be modified and extended to more accurately emulate observed phenomena and make more realistic predictions. The future of the modeling effort will continue to develop and refine predictions regarding glioma prognosis, progression, and therapeutic efficacy.

However, these preliminary data do suggest that these biomathematical modeling techniques provide a novel tool for linking data from disparate sources. In the case of this article, the disparate sources are multimodality imaging observations of individual GBM patients. At first glance, these images may appear relatively distinct and separated by technical (imaging) and biological (modeling) mechanisms; however, the techniques discussed in this article provide a forum for communicating across this multimodality divide. It is clear that such a multimodality analysis can provide valuable insight into a quantitative understanding of the kinetics and pathophysiology of each glioma that could uniquely be used in guiding and assessing the effects of treatment in individual patients.

Disclosure of Potential Conflicts of Interest

No potential conflicts of interest were disclosed.

Acknowledgments

Received 10/6/08; revised 2/26/09; accepted 3/23/09; published OnlineFirst 4/14/09.

Grant support: We gratefully acknowledge the support of the McDonnell Foundation and NIH grant CA042045-20.

The costs of publication of this article were defrayed in part by the payment of page charges. This article must therefore be hereby marked *advertisement* in accordance with 18 U.S.C. Section 1734 solely to indicate this fact.

References

1. Swanson KR, Alvord EC, Jr., Murray JD. Virtual brain tumours (gliomas) enhance the reality of medical imaging and highlight inadequacies of current therapy. Br J Cancer 2002;86:14–8.
2. Stupp R, Mason WP, van den Bent MJ, et al. Radiotherapy plus concomitant and adjuvant temozolomide for glioblastoma. N Engl J Med 2005;352:987–96.
3. Stupp R, Hegi ME, Gilbert MR, Chakravarti A. Chemoradiotherapy in malignant glioma: standard of care and future directions. J Clin Oncol 2007;25:4127–36.
4. Silbergeld DL, Rostomily RC, Alvord EC, Jr. The cause of death in patients with glioblastoma is multifactorial: clinical factors and autopsy findings in 117 cases of supratentorial glioblastoma in adults. J Neurooncol 1991;10:179–85.
5. Mankoff DA, Peterson LM, Tewson TJ, et al. [18F]fluoroestradiol radiation dosimetry in human PET studies. J Nucl Med 2001;42:679–84.
6. Tewson TJ, Krohn KA. PET radiopharmaceuticals: state-of-the-art and future prospects. Semin Nucl Med 1998;28:221–34.
7. Varagnolo L, Stokkel MP, Mazzi U, Pauwels EK. 18F-labeled radiopharmaceuticals for PET in oncology, excluding FDG. Nucl Med Biol 2000;27:103–12.
8. Phelps ME. PET: the merging of biology and imaging into molecular imaging. J Nucl Med 2000;41:661–81.
9. Spence AM, Muzi M, Swanson KR, et al. Regional hypoxia in glioblastoma multiforme quantified with [18F]fluoromisonidazole positron emission tomography before radiotherapy: correlation with time to progression and survival. Clin Cancer Res 2008;14:2623–30.
10. Rasey JS, Grunbaum Z, Magee S, et al. Characterization of radiolabeled fluoromisonidazole as a probe for hypoxic cells. Radiat Res 1987;111:292–304.
11. Rajendran JG, Wilson DC, Conrad EU, et al. [(18)F]FMISO and [(18)F]FDG PET imaging in soft tissue sarcomas: correlation of hypoxia, metabolism and VEGF expression. Eur J Nucl Med Mol Imaging 2003;30:695–704.
12. Rajendran JG, Mankoff DA, O'Sullivan F, et al. Hypoxia and glucose metabolism in malignant tumors: evaluation by [18F]fluoromisonidazole and [18F]fluorodeoxyglucose positron emission tomography imaging. Clin Cancer Res 2004;10:2245–52.
13. Tsang RW, Fyles AW, Milosevic M, et al. Interrelationship of proliferation and hypoxia in carcinoma of the cervix. Int J Radiat Oncol Biol Phys 2000;46:95–9.
14. Brown JM. Therapeutic targets in radiotherapy. Int J Radiat Oncol Biol Phys 2001;49:319–26.
15. Fyles AW, Milosevic M, Wong R, et al. Oxygenation predicts radiation response and survival in patients with cervix cancer. Radiother Oncol 1998;48:149–56.
16. Kleihues P, Ohgaki H. Primary and secondary glioblastomas: from concept to clinical diagnosis. Neuro-oncol 1999;1:44–51.
17. Dachs GU, Tozer GM. Hypoxia modulated gene expression: angiogenesis, metastasis and therapeutic exploitation. Eur J Cancer 2000;36:1649–60.
18. Swanson KR, Bridge C, Murray JD, Alvord EC, Jr. Virtual and real brain tumors: using mathematical modeling to quantify glioma growth and invasion. J Neurol Sci 2003;216:1–10.
19. Swanson KR. Mathematical modeling of the growth and control of tumors [PhD]: University of Washington; 1999.
20. Swanson KR, Rostomily RC, Alvord EC, Jr. A mathematical modelling tool for predicting survival of individual patients following resection of glioblastoma: a proof of principle. Br J Cancer 2008;98:113–9.

21. Murray JD. Mathematical biology I: an introduction. 3rd ed. New York: Springer-Verlag; 2002.

22. Burgess PK, Kulesa PM, Murray JD, Alvord EC, Jr. The interaction of growth rates and diffusion coefficients in a three-dimensional mathematical model of gliomas. J Neuropathol Exp Neurol 1997;56:704–13.

23. Swanson KR, Alvord EC, Jr., Murray JD. A quantitative model for differential motility of gliomas in grey and white matter. Cell Prolif 2000;33:317–29.

24. Mandonnet E, Delattre JY, Tanguy ML, et al. Continuous growth of mean tumor diameter in a subset of grade II gliomas. Ann Neurol 2003;53:524–8.

25. Swanson KR, Alvord EC, Jr. A biomathematical and pathological analysis of an untreated glioblastoma. Helsinki (Finland): 7th European Congress of Neuropathology; 2002.

26. Pallud J, Mandonnet E, Duffau H, et al. Prognostic value of initial magnetic resonance imaging growth rates for World Health Organization grade II gliomas. Ann Neurol 2006;60:380–3.

27. Harpold HL, Alvord EC, Jr., Swanson KR. The evolution of mathematical modeling of glioma proliferation and invasion. J Neuropathol Exp Neurol 2007; 66:1–9.

28. Lim JL, Berridge MS. An efficient radiosynthesis of [18F]fluoromisonidazole. Appl Radiat Isot 1993;44: 1085–91.

29. Swanson KR, Chakraborty G, Wang CH, et al. Complementary but distinct roles for MRI and 18F-fluoromisonidazole PET in the assessment of human glioblastomas. J Nucl Med 2009;50:36–44.

30. Ashburner J, Flandin G, Henson R, et al. Statistical Parametric Mapping (SPM). Functional Imaging Laboratory. 5th ed. Wellcome Department of Imaging Neuroscience: Institute of Neurology; 2005.

31. MATLAB. 2007a edition. Natick (MA): The MathWorks, Inc.; 2007.

32. Rajendran JG, Krohn KA. Imaging tumor hypoxia. In: Bailey DL, Townsend DW, Valk PE, Maisey MN, editors. Positron emission tomography, principles and practice. London: Springer-Verlag; 2002. p. 689–96.

33. Anderson AR, Weaver AM, Cummings PT, Quaranta V. Tumor morphology and phenotypic evolution driven by selective pressure from the microenvironment. Cell 2006;127:905–15.

34. Silva AC, Carvalho PC, Gattass M. Diagnosis of lung nodule using semivariogram and geometric measures in computerized tomography images. Comput Methods Programs Biomed 2005;79:31–8.

35. Kleihues P, Louis DN, Scheithauer BW, et al. The WHO classification of tumors of the nervous system. J Neuropathol Exp Neurol 2002;61:215–25; discussion 26–9.

36. Cher LM, Murone C, Lawrentschuk N, et al. Correlation of hypoxic cell fraction and angiogenesis with glucose metabolic rate in gliomas using 18F-fluoromisonidazole, 18F-FDG PET, and immunohistochemical studies. J Nucl Med 2006;47:410–8.

37. Rasey JS, Nelson NJ, Chin L, Evans ML, Grunbaum Z. Characteristics of the binding of labeled fluoromisonidazole in cells *in vitro*. Radiat Res 1990;122:301–8.

38. Rasey JS, Koh WJ, Evans ML, et al. Quantifying regional hypoxia in human tumors with positron emission tomography of [18F]fluoromisonidazole: a pretherapy study of 37 patients. Int J Radiat Oncol Biol Phys 1996;36:417–28.

39. Brizel DM, Dodge RK, Clough RW, Dewhirst MW. Oxygenation of head and neck cancer: changes during radiotherapy and impact on treatment outcome. Radiother Oncol 1999;53:113–7.

40. Lally BE, Rockwell S, Fischer DB, Collingridge DR, Piepmeier JM, Knisely JP. The interactions of polarographic measurements of oxygen tension and histological grade in human glioma. Cancer J 2006;12:461–6.

41. Swanson KR, Alvord EC, Jr., Murray JD. Dynamics of a model for brain tumors reveals a small window for therapeutic intervention. Discrete Cont Dyn B 2004;4: 289–95.

42. Dence CS, Ponde DE, Welch MJ, Lewis JS. Autoradiographic and small-animal PET comparisons between 18F-FMISO, 18F-FDG, 18F-FLT and the hypoxic selective 64Cu-ATSM in a rodent model of cancer. Nucl Med Biol 2008;35:713–20.

43. Churchill SW, Zajic SC. Prediction of fully developed turbulent convection with minimal explicit empiricism. AIChE J 2002;48:927–40.